

Catalytic oxidation of nitrogen monoxide over $\text{La}_{1-x}\text{Ce}_x\text{CoO}_3$ perovskites

Yuxin Wen^a, Changbin Zhang^a, Hong He^{a,*}, Yunbo Yu^a, Yasutake Teraoka^b

^aState Key Laboratory of Environmental Chemistry and Ecotoxicology, Research Center for Eco-Environmental Sciences, Chinese Academy of Sciences, Beijing 100085, China

^bDepartment of Energy and Material Sciences, Faculty of Engineering Sciences, Kyushu University, Kasuga, Fukuoka 816-8580, Japan

Available online 20 July 2007

Abstract

This paper presents an investigation on the NO oxidation properties of perovskite oxides. $\text{La}_{1-x}\text{Ce}_x\text{CoO}_3$ ($x = 0, 0.05, 0.1, 0.2, 0.3, 0.4$) perovskite-type oxides were synthesized through a citrate method and characterized by XRD, BET and XPS. The catalytic activities were enhanced significantly with Ce substitution, and achieved the best when x was 0.2, but decreased at higher x values. The performed characterizations reveal that the adsorbed oxygen on the surface plays an important role in the oxidation of NO into NO_2 . The surface compounds after the co-adsorption of NO and O_2 at room temperature, were investigated by DRIFTS and TPD experiments. Three species: the bridging nitrate, the hyponitrites and the monodentate nitrate, were formed on the surface. The order of thermal stabilities was as follows: monodentate > hyponitrite > bridging. Among them, only the monodentate nitrate which decomposed at above 300 °C, would desorb NO_2 into the gas phase. When Ce was added, the temperature of monodentate nitrate desorption became low and the adsorption of the other two species decreased. This might be related to the oxidation state of Co on the surface. Analysis by synthesizing the characterization results and catalytic activity data shows that large amounts of adsorbed oxygen, small amount of inactive compounds on the surface and low NO_2 desorption temperature are favorable for the oxidation of NO.

© 2007 Elsevier B.V. All rights reserved.

Keywords: Perovskite; NO oxidation; $\text{La}_{1-x}\text{Ce}_x\text{CoO}_3$; TPD; DRIFTS; Nitrate

1. Introduction

Extensive studies on the NO_x catalytic elimination have been carried out for years. However, the removal of NO_x from diesel engines and a lean-burn condition of gasoline engines with the presence of excess oxygen is still a challenge. NO_2 is always more favored than NO for NO_x conversion among the several developed procedures under oxidizing conditions, such as the technique of NO_x storage and reduction (NSR) [1], the continuously regenerated trap (CRT) technology for the simultaneous NO_x and soot removal [2], and the selective catalytic reduction (SCR) of NO_x , especially with some N-contained species as agents like ammonia or urea [3–5]. We also found that formation of NO_2 is an essential step in the mechanism of the SCR of NO by hydrocarbons [6,7]. Some researchers have also developed several more complicated systems, such as the “VHRO-system” (V = oxidizing catalyst for NO to NO_2 , H = hydrolyzing catalyst, R = SCR catalyst,

O = oxidizing catalyst for NH_3) [5] and the IAR (the Intermediate Addition between an oxidation and a reduction catalyst of reductant) method [8]. In these systems, they all set a pre-catalyst for the oxidation of NO before adding the reductant, and the efficiency of reductant is significantly improved. In conclusion, there is considerable interest in developing the catalysts for oxidizing NO into NO_2 .

The platinum-based catalysts are most commonly used now for the oxidation of NO. Després Joël et al. observed that Pt/ SiO_2 (2.5 wt.%) could convert about 80% of NO to NO_2 at 300 °C [9]. And a higher NO oxidation rate was observed for larger platinum particles and higher loading of platinum by Xue et al. [10]. However, high cost of the noble metal limits its application.

Catalytic applications of perovskite-type oxides (general formula: ABO_3) have been studied extensively since 1970. A great many elements can be involved in the ABO_3 type crystal structure with a high thermal stability. By partial substitution of ions in site A and/or site B, one can regulate the amount of structure defects and the valence distribution of the B-site ion in the material. These excellent characteristics of perovskite-type oxides make them suitable catalysts for many reactions, i.e.,

* Corresponding author. Tel.: +86 10 62849123; fax: +86 10 62923563.
E-mail address: honghe@rcees.ac.cn (H. He).

oxidation of CO or hydrocarbons, NO_x decomposition, hydrogenation and so on [11,12]. However, as far as we know, none of their application in oxidation of NO has ever been published. In this study, a series of La_{1-x}Ce_xCoO₃ perovskite-type catalysts, with *x* ranging from 0 to 0.4, were synthesized. Their high activities for the oxidation of NO were observed and their characterizations by XRD and TPD were presented here. Compared with the noble metal catalysts, the perovskite catalyst attracts more attention for its low cost, high catalytic activity and high thermal stability.

2. Experimental

2.1. Catalyst preparation

La_{1-x}Ce_xCoO₃ (*x* = 0, 0.05, 0.1, 0.2, 0.3, 0.4) perovskites were prepared by the citrate method. La(NO₃)₃·6H₂O, Ce(NO₃)₃·6H₂O, Co(NO₃)₂·6H₂O in appropriate quantities were dissolved in distilled water. Citric acid monohydrate was then added into the mixture in 10 wt.% excess over the stoichiometric quantity to assure the complexation of metal ions. Water was removed on a rotary evaporator at 80 °C until a viscous gel was formed. The gel was dried overnight in a vacuum oven set at 100 °C, and the spongy, highly hygroscopic, amorphous precursor was obtained. The precursor was then milled and calcined in air at 700 °C for 2 h to obtain the perovskite oxides. The samples were pressed, crushed, and sieved to 20–40 mesh to obtain the suitable particles for experiments.

2.2. Catalyst characterization

Phase identification of the fresh catalysts was carried out by X-ray diffractometry using a computerized Rigaku D/max-RB X-ray diffractometer (Japan, Cu Kα radiation, 0.154056 nm). Diffractograms were recorded with a step scan of 0.02° for 2θ between 15° and 75°. Phase recognition was obtained by comparison with JCPDS files. The nitrogen adsorption–desorption isotherms were obtained at –196 °C over the whole range of relative pressures, using a Micromeritics ASAP 2100 automatic equipment. Specific surface areas were computed from these isotherms by applying the BET method. X-ray photoelectron spectroscopy (XPS) analyses were performed on a MKII (Thermo VGScientific) with a monochromatized microfocused Al X-ray source. The analyzer pass energy was 50 eV. The spectra were measured in vacuum, better than 10⁻¹⁰ mbar. The spectra of C 1s, O 1s, La 3d, Co 2p, and Ce 3d were recorded. The charge correction was made considering that the C 1s signal of contaminating carbon (C–C or C–H bonds) was centered at 284.9 eV.

Temperature-programmed desorption (TPD) experiments were performed in a quartz reactor with a quadruple mass spectrometer as a detector. One hundred and fifty milligram catalyst sample (20–40 mesh) was used in each analysis. The total gas flow of the TPD system was fixed at 30 ml/min. In order to remove water and possible hydrocarbon from the surface of catalyst, the sample was pretreated in a flow of 8%

O₂/He at 600 °C for 1 h and then cooled down to room temperature in pure helium. For the NO and O₂ TPD experiments, the feed was a mixture of 800 ppm NO and 8% O₂, balanced with helium. After the adsorption completed, the system was thoroughly flushed for 2 h with pure helium. Finally, the catalysts were ramped to 600 °C at a heating rate of 30 °C/min. The composition of the desorbed gas was continuously monitored by the mass spectrometer.

In situ DRIFTS spectra were recorded with a NEXUS 670-FTIR equipped with a smart collector and a liquid N₂ cooled MCT detector. All spectra were measured with a resolution of 4 cm⁻¹ and accumulating 100 scans. The catalyst samples were finely ground and placed in a ceramic crucible. The DRIFTS spectra were recorded following the same procedure as TPD experiments. Different spectra at corresponding temperatures obtained from He treated sample were used as reference.

2.3. Catalytic activity valuation

The catalysts (2 g, 20–40 mesh) were tested in a fixed bed quartz tubular reactor operated at atmospheric pressure. The reaction gas contained 800 ppm NO, 8% O₂ and helium as the balance. The total flow rate was 1250 ml/min. The composition of the product gas was analyzed by using gas chromatograph (Agilent 6890) and a chemiluminescence NO_x analyzer (Ecotech, ML 9841s). A molecular-sieve 5 Å column and a Porapak Q column were used to quantify the N₂, O₂ and N₂O in the gas flow. All the test data were confirmed by an FT-IR spectrometer (Nicolet NEXUS 670), which was equipped with a multireflection gas cell (Nicolet, optical path length = 10 m).

The conversion of NO, *X* (%), is defined as the percentage of NO feed that has reacted

$$X (\%) = \frac{(\text{NO})_{\text{in}} - (\text{NO})_{\text{out}}}{(\text{NO})_{\text{in}}} \times 100.$$

3. Results and discussion

3.1. Structural features of catalysts

Fig. 1 shows the structural characteristics of the catalysts with different compositions. From the XRD patterns, we can find that the perovskite phase was fully formed in all the samples. It is indicated that the calcination condition (2 h at 700 °C) is sufficient to give well-crystallized ABO₃ type perovskite structure. On the other hand, similar to the results in refs. [13–15], substitution of cerium with increasing values resulted in the appearance of additional phases and a change of perovskite structure itself. For *x* = 0 and 0.05, the structures were the rhombohedral LaCoO₃-type (JCPD-ICDD 25-1060); when *x* ≥ 0.1, the samples exhibited the pattern of cubic LaCoO₃ (JCPD-ICDD 75-0279). This is indicated by the clearly merge of two close reflections (2θ = 32.9 and 33.2°) into one peak [13]. The solubility of cerium in the perovskite structure was low. With the addition of cerium, a mixed phase

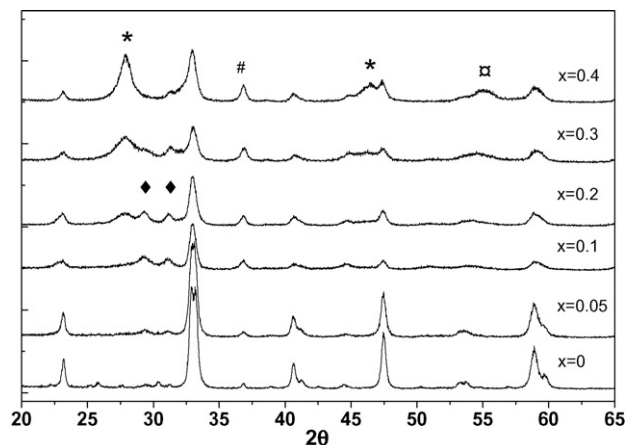


Fig. 1. XRD profiles of $\text{La}_{1-x}\text{Ce}_x\text{CoO}_3$ calcined at 700°C for 2h: (*) Ce_6O_{11} ; (□) CeO_2 ; (#) Co_3O_4 ; (◆) La_2CoO_4 .

of catalyst was expected. As shown in Fig. 1, only when $x > 0.1$, the peaks of Co_3O_4 (JCPD-ICDD 42-1467), La_2CoO_4 (JCPD-ICDD 34-1081), CeO_2 (JCPD-ICDD 43-1002) and Ce_6O_{11} (JCPD-ICDD 32-0196) were observed, and the intensities increased with x . It can be concluded that the solubility of cerium in these samples was limited to $x \leq 0.1$.

3.2. Specific surface area

BET results of the catalysts are shown in Table 1. The specific surface areas (SSA) of $\text{La}_{1-x}\text{Ce}_x\text{CoO}_3$ catalysts were relatively low, about $9\text{--}12\text{ m}^2/\text{g}$, which is in agreement with ref [13]. Calcination at high temperature is necessary to obtain the perovskite-type oxide catalyst, but such treatment often results in a dramatic decrease in the specific surface area. It is also notable that the substituted samples have a larger SSA than LaCoO_3 . However, the enhancement was not linear with the substitution. When cerium addition was below its solubility in perovskite structure, a significant increase in SSA appeared; when x is larger than 0.1, with the increased proportion of additional phases as shown in XRD profiles, their SSA decreased in some extent.

3.3. Catalytic activity

Fig. 2 presents the conversions of NO as a function of the reaction temperature over $\text{La}_{1-x}\text{Ce}_x\text{CoO}_3$ catalysts. Each datum point is the average of measurements at steady state. NO was converted to NO_2 and neither N_2 nor N_2O was detected.

Table 1
Results of specific surface area ($\text{m}^2\text{ g}^{-1}$) of $\text{La}_{1-x}\text{Ce}_x\text{CoO}_3$ calcined at 700°C for 2 h

x	SSA ($\text{m}^2\text{ g}^{-1}$)
0	8.9
0.05	11.4
0.1	12.6
0.2	11.0
0.3	9.8
0.4	10.8

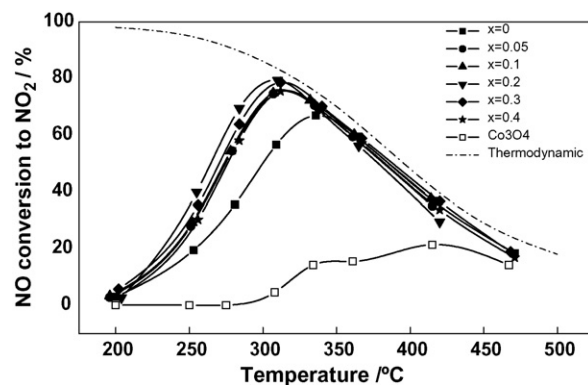


Fig. 2. Activities of $\text{La}_{1-x}\text{Ce}_x\text{CoO}_3$ for NO oxidation. Reaction conditions: NO 800 ppm, O_2 8%, He balance, total flow rate: 1250 ml/min, W/F: 0.096 g s/ml.

At low temperatures the oxidation of NO was kinetically limited. With the temperature rising, the activity was increased, and the thermodynamic limit (the dot line [5]) was achieved. In the case of perovskite samples, ever since the addition of cerium, large enhancement of the activity for NO oxidation was observed and the maximum activity point moved to lower temperature. The sample with $x = 0.2$ got the best performance, about 80% conversion at 300°C . The catalytic activity drew back for a higher degree of cerium substitution. Compared with the perovskite-type oxides, the activity of pure Co_3O_4 was low, and CeO_2 did not even show any activity for NO oxidation, which is not mentioned in this figure. The additional phases would not contribute much to the catalytic activity directly. On the other hand, according to the report of Kirchnerova [13], there might be a cooperation effect existing among the mixed phases. The interfaces between different phases might produce some deficient structures, and accelerated the activities to some extent. However, the promotion mechanism is still not clearly explained, and more works would be needed in the future.

3.4. X-ray photoelectron spectroscopy

For catalytic reaction, the surface characteristics are always more important than lattice. Thus, the XPS was used to reveal the chemical state and the relative abundance of the elements on the surface of $\text{La}_{1-x}\text{Ce}_x\text{CoO}_3$ catalysts. The binding energy values of La $3d_{5/2}$ were recorded at 837.7 and 834.4 eV. These are similar to the values recorded from pure lanthana. It indicated that lanthanum ions were present in the trivalent form. No change of the binding energy was detected when lanthanum was substituted with cerium.

The Co 2p signal is a typical distorted peak of Co^{3+} , which results from complex state effects (Fig. 3). In all the samples no clearly satellite peaks in the 785–788 eV are observed, which indicates Co^{3+} is dominant in all the samples [16]. However, because of the spectrum over-lapping, it is hard to clearly distinguish Co^{2+} from Co^{3+} . Slight shifts in the binding energies of Co $2p_{3/2}$ were found with increasing x . For $x = 0.05, 0.1$ and 0.2 , the Co $2p_{3/2}$ peak moved from 779.6 eV ($x = 0$) to 780.3 eV, immediately. When $x = 0.3$ and 0.4 , the peak shifted

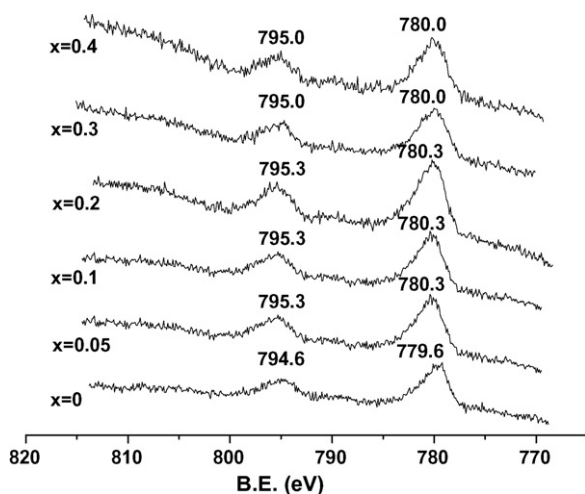


Fig. 3. Co 2p XPS spectra of $\text{La}_{1-x}\text{Ce}_x\text{CoO}_3$ catalysts.

back to 780.0 eV. This chemical shift reveals the partially varying of cobalt valence. As recorded by Moudler, pure Co_2O_3 exhibits a peak centred at 779.9 eV, and pure CoO shifts to 780.4 eV [17]. Taguchi also reported that the increasing of Co^{2+} ion content induced the shift toward the high binding energy site [18]. In this case of $\text{La}_{1-x}\text{Ce}_x\text{CoO}_3$, when tetravalent Ce ions were fully dissolved into the perovskite structure ($x \leq 0.1$), an electronic unbalance was generated. As a result, a part of trivalent Co in the B-site became divalent to preserve the charge neutrality. On the other hand, when the cerium addition exceeded the solution limits ($x > 0.1$), the peaks of CeO_2 phase appeared in XRD. Nitadori et al. [19] reported that, in $\text{La}_{1-x}\text{Ce}_x\text{CoO}_3$, an A-cation deficient perovskite might be generated, and the trivalent Co ion was suggested to be partly changed into tetravalent state. In our case, it is notable that there is Co_3O_4 phase generated at the same time. Therefore, we cannot directly draw the same conclusion as Nitadori did. However, we did observe the Co valence state increase because the binding energy of Co shifted back with the increasing proportion of Ce.

Fig. 4 shows the XPS spectra of O 1s. According to the reference [20], the O 1s peak was curve-fitted with three kinds of Gaussian peaks: lattice O^{2-} at 529.2 eV, adsorbed oxygen such as O^- or OH^- at 531.4–531.6 eV, and adsorbed molecular water at above 533.2 eV [21].

The surface atomic ratio obtained from XPS was summarized in Table 2. In all of the samples, the La/Co and Ce/Co ratio are both significantly larger than the theoretical ones, suggesting the surface enrichment of A-site elements. This phenomenon was commonly observed for perovskite oxides, and no remarkable connection with their catalytic activities was observed [22]. On the other hand, it is generally accepted that the adsorbed surface oxygen often participates in oxidation reactions. Among the substituted catalysts, the sample ($x = 0.2$) which showed the best activity for NO oxidation achieved the highest percentage of adsorption oxygen, as shown in Table 2. Definitely the adsorbed oxygen played an important role in the oxidation of NO. However, the perovskite LaCoO_3 which also got high amount of adsorbed

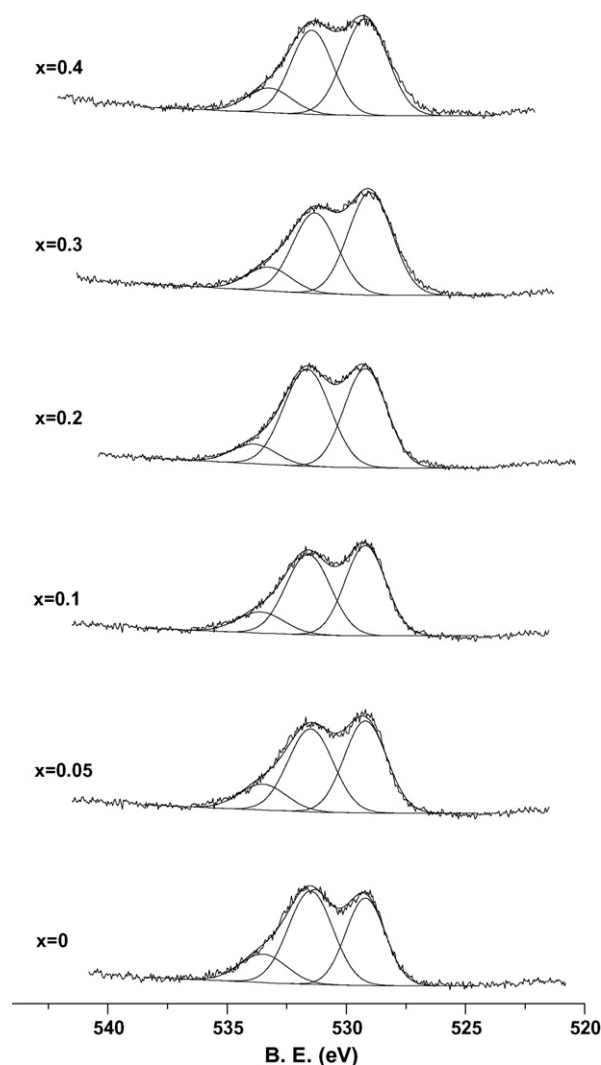


Fig. 4. O 1s XPS spectra of $\text{La}_{1-x}\text{Ce}_x\text{CoO}_3$ catalysts.

Table 2
The surface atomic ratio obtained from XPS

x	La/Co	Ce/Co	Co/La+Ce+Co	O (%)	O 1s ^a
0.0	1.73	0	0.37	68.98	529.2 (38.5)
					531.5 (46.6)
					533.5 (14.9)
0.05	1.48	0.11	0.39	70.11	529.2 (44.2)
					531.5 (42.2)
					533.5 (13.6)
0.1	1.61	0.16	0.36	71.28	529.2 (44.6)
					531.6 (43.5)
					533.6 (11.9)
0.2	1.47	0.34	0.36	71.03	529.2 (43.4)
					531.6 (48.4)
					533.3 (8.2)
0.3	1.68	0.45	0.32	71.47	529.2 (48.2)
					531.5 (39.8)
					533.2 (12.0)
0.4	1.34	0.67	0.33	74.93	529.2 (49.6)
					531.4 (38.3)
					533.2 (12.1)

^a The value in parenthesis is the peak percentage (%) of the corresponding oxygen species in the total surface oxygen obtained from the fitting of O 1s XPS spectra.

oxygen had a low activity. It indicates that the catalytic activities of samples are not simply determined by adsorbed oxygen amount, and this will be further discussed in the following parts.

3.5. TPD and DRIFTS study of NO and O₂ co-adsorption and desorption

To elucidate the reaction mechanism, it is important to study the surface compounds under reaction conditions. The catalysts were saturated in a flow of NO + O₂ + He at room temperature before the TPD experiments were carried out. The NO, O₂, N₂O and N₂ TPD results of all the samples were similar. As a typical one, the TPD spectra of La_{0.6}Ce_{0.4}CoO₃ are shown in Fig. 5. In all the experiments, no N₂ signal was detected, which indicated no directly decomposition of NO occurred on the surface. Weak signals of N₂O desorption were recorded with peak temperatures at 250 °C over Ce doped samples while it is not observed in the case of pure LaCoO₃. Therefore, the formation of N₂O was evidently due to the cerium addition. This will be further discussed later. All of the samples show two major NO desorption peaks along the TPD processes. More importantly, along with the second peak of NO, O₂ signal was detected with a proportional amount of NO. This observation is similar with the records by Forni et al. [15]. It could be concluded that NO₂ was desorbed above 250 °C, and the detections of both NO and O₂ were due to the fractions of NO₂ molecular bombed by electron beam in the QMAS chamber.

The NO profiles of all samples are combined in Fig. 6. From this figure, we could find that the desorption amount of NO decreased with the increase of Ce doping. At the same time, desorption temperature of NO₂ became lower. For better understanding of the nature of NO_x desorption and surface species on catalysts, DRIFTS experiments were performed.

The DRIFTS spectra were taken at steady states under the same conditions as NO_x TPD experiments. In this case, it can be assumed that equilibrium was reached on the surface.

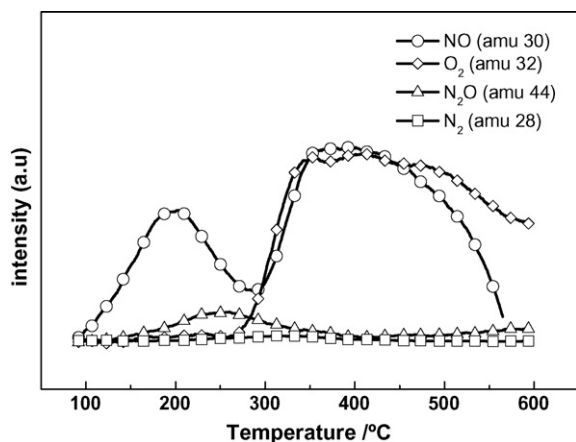


Fig. 5. Typical NO, N₂O, N₂ and O₂ TPD spectra of La_{0.6}Ce_{0.4}CoO₃ sample after exposure to a flow of NO (800 ppm)/O₂ (8%)/He at room temperature for 1 h. TPD conditions: He flow (30 ml/min) with heating to 600 °C at a rate of 30 °C/min.

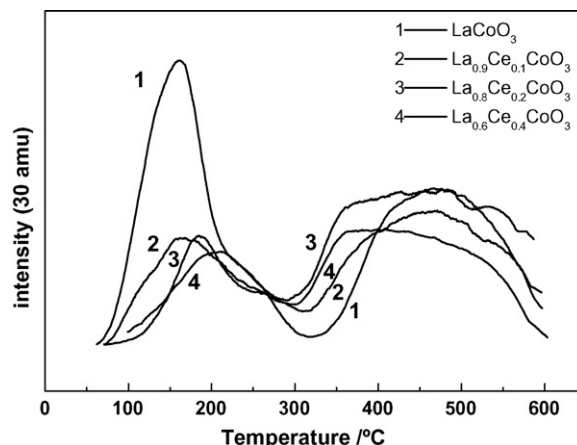


Fig. 6. NO TPD profiles of La_{1-x}Ce_xCoO₃ catalysts after exposing to a flow of NO (800 ppm)/O₂ (8%)/He at room temperature for 1 h. TPD conditions: He flow (30 ml/min) with heating to 600 °C at a rate of 30 °C/min.

Therefore, only the adsorption species with high stabilities left on the surface before the spectra were taken.

Fig. 7 shows the dynamic changes in the DRIFTS spectra of La_{0.6}Ce_{0.4}CoO₃ as a function of temperature in a flow of He after saturated the catalyst in a flow of NO + O₂ + He mixture gas at room temperature. According to the literature [23,24], band at 1643 cm⁻¹ can be assigned to the bridging nitrate. The 1419, 1344, 1059 and 857 cm⁻¹ bands can be assigned, respectively, to *trans*- and *cis*-hyponitrite (N₂O₂²⁻) species. Bands at 1542 and 1305 cm⁻¹ should be assigned to monodentate nitrates.

On the basis of the TPD and DRIFTS results, we found that the three species on the surface have different thermal stability. As the temperature increased, the bridging nitrates disappeared

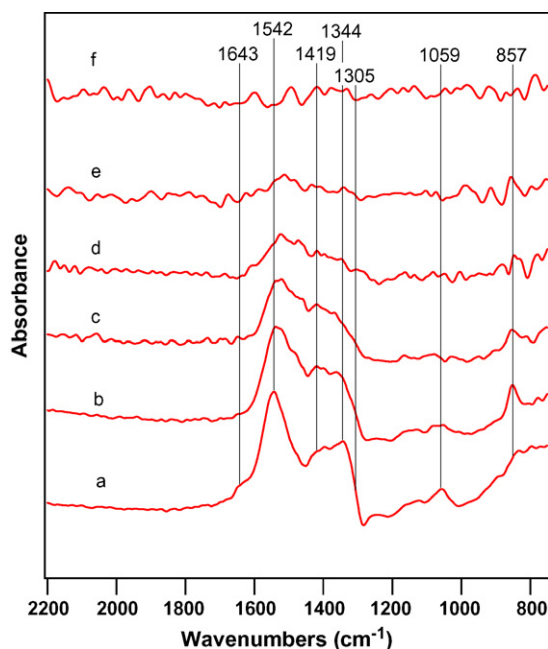


Fig. 7. DRIFTS spectra of the La_{0.6}Ce_{0.4}CoO₃ sample as a function of temperature. Catalyst was pre-saturated in a flow of NO (800 ppm)/O₂ (8%)/He mixture, at 30 °C. Spectra a, b, c, d, e and f were collected in flowing He at 30, 100, 150, 200, 250 and 300 °C, respectively.

around 100 °C contributing the low temperature NO desorption observed in the TPD profiles. The monodentate nitrate at 1543 and 1305 cm⁻¹ band was the stablest species on the surface, and can be detected even at 300 °C, then decomposed and desorbed as NO₂ into the gas phase [25].

The hyponitrite species were stable up to 250 °C and then disappeared at higher temperature. The corresponding compounds observed in TPD experiment were NO and N₂O. Martinez-Arias et al. [24] reported that the hyponitrites could decompose to produce N₂O on CeO₂. According to the XRD results as shown in Fig. 1, the additional phase, CeO₂, would appear when x in La_{1-x}Ce_xCoO₃ was bigger than 0.2 because the cerium solubility in the perovskite structure was very low. This might result in the formation of N₂O. Furthermore, in the case of LaCoO₃, no cerium was added, and then no N₂O was detected. It is also notable that during the activity tests, no remarkable N₂O was detected. This may be due to its low concentration or change of reaction conditions.

On the basis of the above results and discussions, we can conclude that only the monodentate nitrate can result in the formation of NO₂ in the gas phase, and therefore plays a key role in the oxidation of NO. The desorption of the monodentate nitrate will regenerate the active sites on the surface and keep the reaction continue. The other NO_x surface species, the bridging nitrate and *trans-cis*-hyponitrite, are not responsible for NO₂ formation. Even more, they may have a negative effect, because they will compete with the monodentate nitrate for the adsorption sites on the surface. The substitution of cerium decreased both the amount of these two species and lowered the desorption temperature of the monodentate nitrate, as shown in Fig. 6. This change may be due to the partially variation of surface conditions as indicated from XPS records.

The catalytic activities of La_{1-x}Ce_xCoO₃ for NO oxidation are most relevant to the decomposition temperatures of monodentate nitrate species which resulted in the desorption of NO₂ into the gas phase. For example, the sample La_{0.8}Ce_{0.2}CoO₃, which decomposed the monodentate nitrates at the lowest temperature, achieved the best performance in the activity of NO oxidation. When x was higher than 0.2, the inactive phases CeO_x and Co₃O₄ appeared, and the adsorbed oxygen amount decreased. The combination of all these factors caused the decrease of activity when $x = 0.3$ and 0.4 .

4. Conclusion

The prepared La_{1-x}Ce_xCoO₃ samples exhibit good activities as regular noble metal catalysts, with the highest conversion of

80% at about 300 °C. The bridging nitrate, hyponitrites and monodentate nitrate were formed on the La_{1-x}Ce_xCoO₃ surface. Experiments show that only the monodentate nitrate resulted in the formation of NO₂ in the gas phase. The presence of cerium decreased the thermal stability of the monodentate nitrate and the amount of the other two nitrate species. The amount of adsorbed oxygen also influenced the NO oxidation reaction. An integration of all these factors resulted in the best performance of the sample when $x = 0.2$.

Acknowledgements

This work was partially supported by the National Natural Science Foundation of China (20621140004) and the Ministry of Science and Technology, China (2004CB719503).

References

- [1] N. Takahashi, H. Shinjoh, T. Iijima, T. Suzuki, K. Yamazaki, H. Ko Yokota, N. Suzuki, S. Miyoshi, T. Matsumoto, T. Tanizawa, S. Tanaka, K. Tateishi, Kasahara, Catal. Today 27 (1996) 63.
- [2] B.J. Cooper and J.E. Thoss, SAE Paper No. 890404, 1989
- [3] F. Nakajima, I. Hamada, Catal. Today 29 (1996) 109.
- [4] M. Richter, A. Trunschke, U. Bentrup, J. Catal. 206 (2002) 98.
- [5] M. Koebel, M. Elsener, M. Kleemann, Catal. Today 59 (2000) 335.
- [6] H. He, J. Wang, Q. Feng, Y. Yu, K. Yoshida, Appl. Catal. B 46 (2003) 365.
- [7] Y. Yu, H. He, Q. Feng, H. Gao, X. Yang, Appl. Catal. B 49 (2004) 159.
- [8] M. Iwamoto, T. Zengyo, A.M. Hernandez, H. Araki, Appl. Catal. B 17 (1998) 259.
- [9] M. Després Joël, M. Elsener, O. Koebel, B. Kröcher, A. Schnyder, Wokaun, Appl. Catal. B 50 (2004) 73.
- [10] E. Xue, K. Seshan, J.R.H. Ross, Appl. Catal. B 11 (1996) 65.
- [11] H. Tanaka, M. Misono, Curr. Opin. Solid State Mater. Sci. 5 (2001) 381.
- [12] M.A. Pena, J.L.G. Fierro, Chem. Rev. 101 (2001) 1981.
- [13] J. Kirchnerova, M. Alifanti, B. Delmon, Appl. Catal. A 231 (2002) 65.
- [14] H. Tanaka, N. Mizuno, M. Misono, Appl. Catal. A 244 (2003) 371.
- [15] L. Forni, C. Oliva, F.P. Vatti, M.A. Kandala, A.M. Ezerets, A.V. Viishniakov, Appl. Catal. B 7 (1996) 269.
- [16] M. Oku, Y. Sato, Appl. Surf. Sci. 55 (1992) 37.
- [17] J.F. Moudler, W.F. Sticle, P.E. Sobol, K.D. Bomben, in: J. Chastain (Ed.), Handbook of XPS, Perkin-Elmer, Eden raine, 1992, p. 219.
- [18] H. Taguchi, H. Kido, K. Tabata, Phys. B 344 (2004) 271.
- [19] T. Nitadori, M. Misono, J. Catal. 93 (1985) 459.
- [20] S. Ponce, M.A. Pena, J.L.G. Fierro, Appl. Catal. B 24 (2000) 193.
- [21] L.G. Tejuca, J.L.G. Fierro, J.M.D. Tascon, Adv. Catal. 36 (1989) 237.
- [22] M. Alifanti, R. Auer, J. Kirchnerova, F. Thyron, P. Grange, B. Delmon, Appl. Catal. B 41 (2003) 71.
- [23] K.I. Hadjiivanov, Catal. Rev. Sci. Eng 42 (1–2) (2000) 71.
- [24] A. Martinez-Arias, J. Soria, J.C. Conesa, X.L. Seoane, A. Arcoya, R. Cataluna, J. Chem. Soc. Faraday Trans. 91 (11) (1995) 1679.
- [25] S. Kameoka, Y. Ukisu, T. Miyadera, Phys. Chem. Chem. Phys. 2 (2000) 367.